A Comparative Study of Rapidly and Slowly Rotating Dynamical Regimes in a Terrestrial General Circulation Model

ANTHONY D. DEL GENIO

NASA/Goddard Space Flight Center, Institute for Space Studies, New York, NY 10025

ROBERT J. SUOZZO

Sigma Data Services Corporation, Institute for Space Studies, New York, NY 10025

(Manuscript received 3 April 1986, in final form 7 October 1986)

ABSTRACT

As a preliminary step in the development of a general circulation model for general planetary use, a simplified version of the GISS Model I GCM has been run at various rotation periods to investigate differences between the dynamical regimes of rapidly and slowly rotating planets. To isolate the dynamical processes, the hydrologic cycle is suppressed and the atmosphere is forced with perpetual annual mean solar heating. All other parameters except the rotation period remain fixed at their terrestrial values. Experiments were conducted for rotation periods of ⅔, 1, 2, 4, 8, 16, 64 and 256 days. The results are in qualitative agreement with similar experiments carried out previously with other GCMs and with certain aspects of one Venus GCM simulation. As rotation rate decreases, the energetics shifts from baroclinic to quasi-barotropic when the Rossby radius of deformation reaches planetary scale. The Hadley cell expands poleward and replaces eddies as the primary mode of large-scale heat transport. Associated with this is a poleward shift of the baroclinic zone and jet stream and a reduction of the equator-pole temperature contrast. Midlatitude jet strength peaks at 8 days period, as does the weak positive equatorial zonal wind which occurs at upper levels at all rotation periods. Eddy momentum transport switches from poleward to equatorward at the same period. Tropospheric mean static stability generally increases in the tropics and decreases in midlatitudes as rotation rate decreases, but the global mean static stability is independent of rotation rate. The peak in the eddy kinetic energy spectrum shifts toward lower wavenumbers, reaching wavenumber 1 at a period of 8 days. Implications of these results for the dynamics of Venus and Titan are discussed. Specifically, it is suggested that the extent of low-level convection determines whether the Gierasch mechanism contributes significantly to equatorial superrotation on these planets.

1. Introduction

The atmospheric dynamics of slowly rotating planets, for which the quasi-geostrophic approximation does not hold, is a poorly understood subject compared to the more thoroughly investigated rapidly rotating and nonrotating cases. Some of the properties of thermally forced slowly rotating fluids are revealed by the classical dishpan experiments, but the cylindrical geometry, unit aspect ratio, and viscous nature of these flows limit their usefulness in a planetary context. (See, however, the recent study of Read, 1986a,b).

Interest in the slowly rotating regime has been spurred by the confirmation of a strong planetwide superrotation of the Venus atmosphere (Counselman et al., 1980; Newman et al., 1984; Limaye, 1985; Rossow, 1985), a result contrary to intuition based on the limit of no rotation. A similar dynamical regime has been inferred from brightness temperatures for Titan (Flasar et al., 1981), whose rotation period is thought to lie between those of Earth and Venus. These planets thus give rise to several important questions: What dynamical processes are responsible for superrotation on slowly rotating planets? Is superrotation an inevitable consequence of slow rotation? At what rotation period does the transition to the slowly rotating regime occur, and is the transition sensitive to other parameters?

Theories for superrotation generally fall into two classes. One view holds that upward and poleward angular momentum transports by the mean meridional circulation produce a barotropically unstable high latitude jet; the resulting equatorward eddy momentum flux maintains the equatorial zonal wind (Gierasch, 1975; Rossow and Williams, 1979). Alternatively, the diurnal and higher harmonics in the solar heating field give rise to either a "moving flame" circulation or thermal tides whose associated horizontal and/or vertical eddy flux convergences may drive the cloud top equatorial wind (Young and Schubert, 1973; Fels and Lindzen, 1974; Pechmann and Ingersoll, 1984; Leovy, 1986). The tidal mechanism has never been properly tested in a full three-dimensional general circulation model (GCM); wave–mean flow interaction models suggest only a limited role for the tides (Baker and

Leovy, 1987). The Gierasch mechanism has been investigated in one Venus GCM simulation (Rossow, 1983) and produced only a very weak superrotation.

Unfortunately, Venus GCMs are limited by the 90-bar thickness of the atmosphere, which necessitates extremely long integration times for approach to equilibrium. Since the reasons for previous failures are not well understood, a reasonable alternative is to use a slowly rotating Earth GCM as an exploratory tool for understanding superrotation in a wider context. Hunt (1979) examined rotation periods five times greater than and less than Earth's, but did not go far enough to qualitatively change the dynamical regime. Williams and Holloway (1982) presented zonal flow patterns for a wide range of rotation periods, including tests of sensitivity to obliquity and diurnal cycle, using a hemispheric 120° sector model with hydrology. Geisler et al. (1983) removed hydrology, radiation, and topography from the NCAR CCM to produce a spherical counterpart to the regime diagram derived from rotating annulus experiments. Covey et al. (1986) used the same model to examine the rotation dependence of equatorial superrotation. The maximum rotation period in any of these experiments was 64 days.

Aside from superrotation, variable rotation GCMs can be used to examine various fundamental issues of dynamic meteorology: What controls the latitudinal extent of the Hadley cell? To what degree do eddies and mean meridional circulations stabilize the lapse rate? What determines the preferred scale of midlatitude eddies? Is atmospheric "efficiency" dependent on dynamical regime? Simple theories have been advanced to answer these questions in a terrestrial context, but each postulates a dependence on rotation rate which has not been thoroughly examined in previous GCM studies.

In this paper, we document a set of variable rotation rate experiments carried out with the GISS GCM as the first step in the development of a version of the model suitable for general planetary use. The simulations at different rotation rates enable us to address each of the basic questions mentioned above by comparing the GCM realization to predictions of simpler models. In addition, by focusing on details of the heat and momentum budgets, we arrive at a possible explanation for the absence of equatorial superrotation in slow rotation GCM experiments. The runs are therefore useful both for the insight they provide on the slowly rotating regime and for the broader context in which they place our understanding of the dynamics of Earth's atmosphere.

2. Model and experiment descriptions

The experiments were conducted with the Model I version of the GISS GCM (Hansen et al., 1983). Model I is a gridpoint model with approximately 8° × 10° horizontal resolution and seven vertical levels with a top at a pressure of 10 mb. The vertical differencing scheme uses the σ-coordinate system. Horizontal differencing uses the schemes of Arakawa (1972) on the B-grid, except that potential temperature replaces temperature as a prognostic variable. The conservation properties of these schemes permit the model to be run with no explicit horizontal or vertical diffusion. The model requires approximately 1.75 hours CPU time per simulated month on the Amdahl 470/V6.

Physics parameterizations for Model I are described fully in Hansen et al. (1983). For the experiments presented here, important features include: 1) radiation, computed with a semi-implicit spectral integration including all significant atmospheric gases, aerosols and cloud particles; 2) dry convection, which mixes heat, moisture and momentum when two adjacent levels are statically unstable; 3) surface fluxes, obtained from a drag-law formulation and a parameterization of the Monin–Obukhov similarity relations.

Before the experiments could be conducted, a suitable control run was needed. From a planetary standpoint, the hydrologic cycle, which plays a central role in Earth's general circulation, is either irrelevant (e.g., Venus) or fundamentally different from that of Earth (e.g., Titan). To simplify the experiments we therefore removed the hydrology by making three changes in the model: 1) ocean heat capacity was set to zero as is done in "swamp model" GCM runs; 2) land ice and sea ice were replaced by surfaces with the albedo of tundra and ocean, respectively; 3) to remove the influence of moist convection, large-scale latent heat release, and variable cloud formation, evaporation was turned off. A control simulation with these changes was run for 21 months with perpetual annual mean solar heating. The effect of shutting off evaporation is to remove gradually most of the water vapor from the atmosphere via precipitation, and ultimately to suppress moist convection and large-scale cloud formation. Statistics were compiled over the final 11 months, by which time global air temperature was changing at a rate ≤ 0.01 K day^{-1}. Comparison with a similar swamp model run including the hydrologic cycle indicates an overall weakening of the general circulation when latent heat forcing is removed and IR opacity reduced, consistent with previous GCM experiments by Rind and Rossow (1984). However, the basic baroclinic nature of the atmospheric energy cycle is preserved, with available potential energy (A) directly supplying most of the eddy kinetic energy (K_E).

Rotation experiments were run for periods of ⅔, 2, 4, 8, 16, 64 and 256 days. The last of these is four times longer than any previously published experiment and comparable to the actual rotation period of Venus (243 days). Each experiment started from the end of month 10 of the control and ran for 4 months (except for the 256 day period case, which was run for an additional month). The adjustment of the circulation to the new rotation rate was essentially completed in 45 days. The

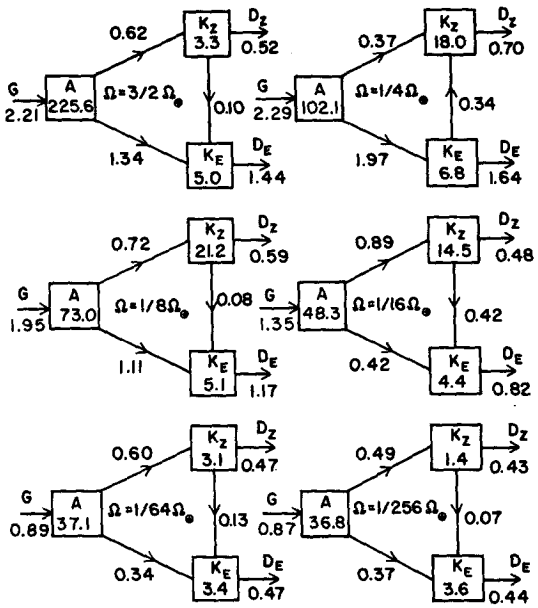

FIG. 1. Atmospheric energy cycle for different rotation rates (Ω) relative to Earth ($\Omega_\oplus$), based on the final 2 months of each experiment. Available potential energy (A), zonal mean kinetic energy (K_Z), and eddy kinetic energy (K_E) in 10^5 J m^{-2}; generation of A (G), dissipation of K_Z (D_Z) and K_E (D_E), and conversions between energy forms (indicated by connecting arrows) in W m^{-2}. G is estimated from the conversions $\{A \cdot K_Z\}$ and $\{A \cdot K_E\}$ and the change in monthly mean A averaged over the final 10 months.

diagnostics presented in this paper represent averages over the final two months of each run. The K_E, K_Z (zonal mean kinetic energy) and A changed during this interval on a time scale at least an order of magnitude longer than the time scale for the forcing and drag.

The perpetual annual mean solar heating imposed in these runs excludes the possibility of thermal tides driving the mean circulation. While tides are potentially important, a realistic assessment of their role on Venus requires accurate diurnal forcing, which is not trivial to mimic in an Earth model because of its much shorter radiative time scale. To sidestep this difficulty, we decided to remove the diurnal cycle in this initial set of experiments. Topography and surface albedo variations and a small variable cloud cover remain, however, generating standing eddies and hemispheric asymmetries. We will show that these effects are small, though, compared to the more fundamental effects of varying the rotation period.

3. Energy cycle

Figures 1–4 illustrate the basic features of the general circulation for the different rotation periods. The effect of varying rotation is perhaps best summarized by the atmospheric energy cycle (Fig. 1). At periods of 2 (not shown) and 4 days, the dynamics is decidedly baroclinic. The K_E is supplied primarily by conversion from

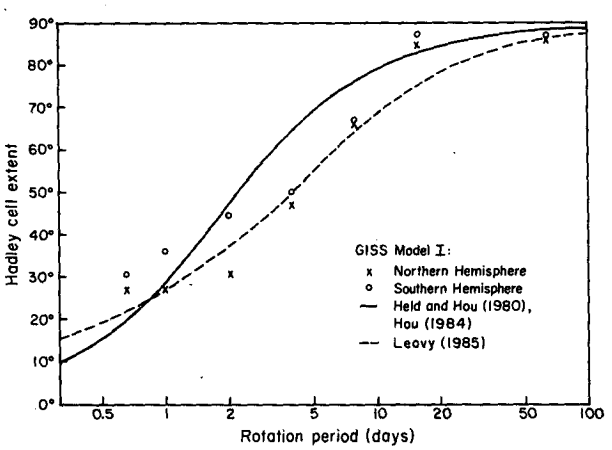

FIG. 2. Latitudinal extent of the Hadley cell in the GCM (defined by change of sign of the 500 mb streamfunction) as a function of rotation period. Plotted for comparison are the predictions of the zonally symmetric analytic model of Held and Hou (1980) and Hou (1984) (for Hadley cell depth 12 km and fractional radiative equilibrium equator–pole temperature contrast ⅓) and of the convective scaling model of Leovy (1985) (for scale height 7 km, radiative relaxation time 0.14 yr, and proportionality constant 1.5). In both cases the parameters are chosen to match the GCM Northern Hemisphere result at 1 day period.

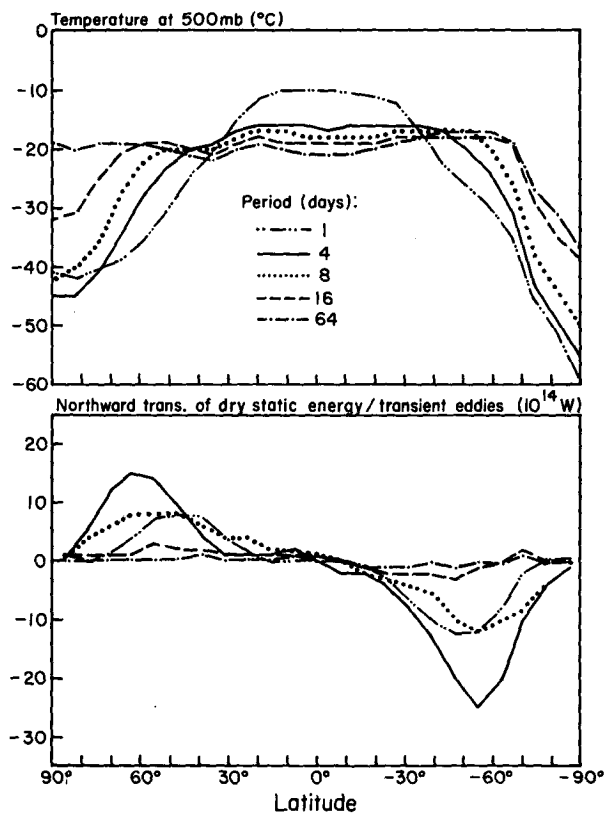

FIG. 3. Latitudinal profiles of zonal mean 500 mb temperature and vertically integrated transient eddy horizontal heat flux for several of the experiments.

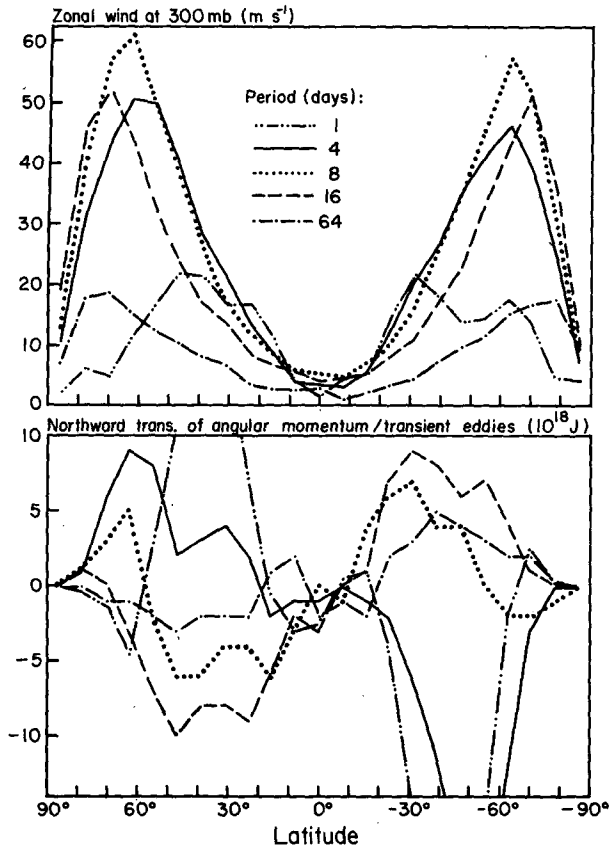

FIG. 4. Latitudinal profiles of zonal mean 300 mb zonal wind and vertically integrated transient eddy horizontal angular momentum flux for several of the experiments.

A; since the heat transport by transient eddies is poleward and correlated with the peak in latitudinal temperature gradient while standing eddies transport heat equatorward (Figs. 3, 8), it is likely that baroclinic instability is responsible. (See also the discussion in section 5.) Conversion of A to K_Z decreases with decreasing rotation rate to a minimum (0.21 W m^{-2}) at 2 days period due to the increasing strength of the midlatitude Ferrel cell. The eddies feed the jet at these periods, since K_E is converted to K_Z; similar behavior is attributed to baroclinic eddies on Earth.

At periods >4 days the dynamics becomes more barotropic. Conversion of A shifts from K_E to K_Z as the Hadley cell strengthens and spreads poleward, eliminating the latitudinal temperature gradient. The K_Z is now converted to K_E and becomes comparable to the baroclinic conversion at 16 days; transient eddy momentum transport is away from jet center and the vorticity field is homogenized equatorward of the jet (Fig. 10), both signs of barotropic instability. Despite this, some baroclinic conversion remains (see section 5) and in fact dominates the barotropic conversion at the longest periods, indicating a weakening of the quasi-barotropic eddies.

At the fastest rotation rates, the dynamics is somewhat less baroclinic than at slightly slower rotation rates. In particular, baroclinic conversion, eddy-to-jet barotropic conversion, Ferrel cell streamfunction magnitude, and K_E all peak at either 2 or 4 days period. If we define atmospheric efficiency as the ratio of total dissipation (surface drag plus convective momentum mixing) to absorbed solar radiation following Lorenz (1960) and note that the latter varies by less than 2% in the experiments, then Fig. 1 implies significant differences. Efficiency peaks at 2 days period (105% of its value in the dry control) and is greatly decreased at both the highest (86%) and lowest (38%) rotation rates. This is consistent with Williams and Holloway (1982), who found that baroclinic eddies peak in efficiency at rotation rates somewhat less than Earth's using a spectral model with effective resolution finer than that of the GISS GCM and different dissipation parameterizations. Thus, there is reason to believe that the peak at 2–4 days represents a real tradeoff between rapid rotation, which inhibits meridional motions, and baroclinicity, which supports such motions. This conflicts with similarity theory applications which predict kinetic energy levels for other planetary atmospheres using scaling analyses which assume roughly constant efficiency (Golitsyn, 1970).

4. Temperature field, mean flow and eddy characteristics

a. Horizontal structure

Figure 2 shows the latitudinal extent of the Hadley cell in both hemispheres for different rotation periods. At short periods, a three-cell circulation exists, but the weak polar cell disappears at 4 days and the Ferrel cell at 64 days, as the Hadley cell spreads poleward monotonically with decreasing rotation rate. (Northern and Southern Hemispheres differ because of different surface albedo fields and topography; in the discussion that follows, quantitative results refer to the Northern Hemisphere unless stated otherwise.)

Figures 3 and 4 show the corresponding behavior of the latitudinal profiles of temperature and zonal wind. The Hadley cell flattens the temperature profile over the latitudes through which it extends by virtue of its net poleward heat transport (Figs. 3, 8). This pushes the baroclinic zone of sharp temperature gradients poleward until it disappears at 64 days. The thermal wind equation then implies that the upper troposphere jet should move poleward at the same rate, which also occurs in the model.

Beyond this zero-order agreement lie some subtle differences, however. Also plotted in Fig. 2 is a prediction of Hadley cell extent based on the symmetric circulation model of Held and Hou (1980) and Hou (1984). Qualitatively, this simple model must agree with the GCM because the Hadley cell must extend to

0° and 90° in the limits of zero and infinite rotation period, respectively. It is clear from Fig. 2, though, that the functional form predicted by Held and Hou is not realized in the GCM. If parameter values for the Held and Hou model are chosen to match the Northern Hemisphere cell in the terrestrial control run, then their model overestimates Hadley cell extent by as much as 15°–20° at intermediate rotation periods while slightly underestimating at ⅔ and 16 days. Similar behavior is seen in the comparison of the Held and Hou model to the experiments of Covey et al. (1986). Comparison of Figs. 2 and 4 indicates that the Hadley cell in the GCM actually ends about 12° equatorward of the jet peak at 4 days, but penetrates poleward of the jet by a similar amount at 16 and 64 days.

These discrepancies can be explained by considering the effect of eddy transports on the mean meridional circulation. In general, negative (positive) latitudinal heating gradients force direct (indirect) circulations, while positive (negative) vertical gradients of momentum sources do the reverse (cf. Rind and Rossow, 1984). At periods of 4 and 8 days, the GCM's eddy heat transports converge at the latitude predicted by Held and Hou for Hadley cell extent (Fig. 3). So too do the eddy angular momentum transports (Fig. 4), but the convergence is primarily in the upper troposphere, providing a vertical gradient of momentum forcing. Both of these tend to force an indirect circulation which offsets the direct thermal forcing by differential insolation at high latitudes. The transition from Hadley to Ferrel cell thus occurs equatorward of the jet peak. Since the GCM eddies are more vigorous at periods slightly longer than one day, the Held and Hou model overestimates Hadley cell extent at these periods when the free parameters are selected to match the observed width on Earth. The weaker model eddies at ⅔ day period have the opposite effect.

On the other hand, at 16 days period, eddy heat fluxes are negligible and eddy angular momentum fluxes mostly equatorward. In this case, the eddies are an angular momentum sink in the upper troposphere at high latitudes. Their forcing enhances the direct thermal circulation and the resulting Hadley cell penetrates slightly farther in latitude, if anything, than the prediction of Held and Hou. At longer periods, the eddies are so weak (Figs. 1, 4) that they have little impact on the mean meridional circulation.

More recently Leovy (1985) has proposed a "convective scaling" model of Hadley cell extent, based on Golitsyn's (1970) similarity theory and the assumption of angular momentum-conserving poleward flow. The prediction of this model is also shown in Fig. 2. In general, agreement with the GCM is somewhat better than for the Held and Hou model. This may be fortuitous, since Leovy assumes that jet speed is independent of rotation, which strongly conflicts with the GCM realization (Fig. 4). As with the Held and Hou model, Hadley cell extent in Leovy's model is less sensitive to rotation rate than the GCM at intermediate periods, again because of the neglect of eddy transport.

b. Vertical structure

Figure 5 shows the latitudinal variation of tropospheric mean static stability for four of the experiments. Because of the depleted water vapor in the model atmosphere, the radiative equilibrium state is statically stable. If we use the Eddington approximation (cf. Goody, 1964, Ch. 8), then the model surface and effective temperatures imply a total optical depth of ~ 1. The tropospheric mean static stability of the radiative equilibrium state (assuming a well-mixed water vapor profile, which is true below 300 mb in the experiments) is then 2.5 K km^{-1}. This is well below the model global mean result of 4.1 K km^{-1}, which varied little with rotation rate despite the change of dynamic regimes.

The latitudinal profile of static stability is sensitive to rotation rate, though, as can be seen from Fig. 5. As rotation rate decreases, equatorial static stability increases. This is a result of the increasingly efficient horizontal heat transport by the Hadley cell, which shifts the burden of balancing the diabatic heating at low latitudes to adiabatic cooling by vertical motions. Since advection of heat is proportional to the potential temperature gradient, such a shift requires decreased horizontal and increased vertical contrasts; this trend is obvious in Figs. 3 and 5. As further proof, the ratio of peak vertical to peak horizontal heat transport in the Hadley cell increases from 0.7 to 2.0 as the rotation period increases from 2 to 64 days.

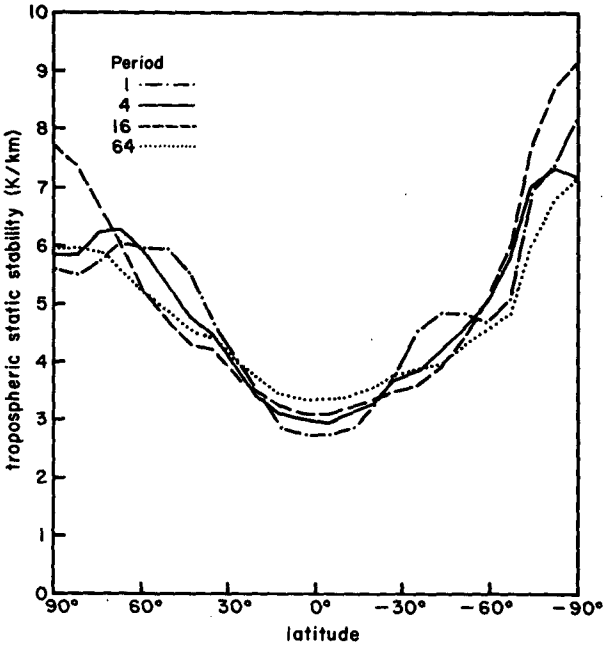

FIG. 5. Tropospheric mean static stability as a function of latitude for several of the experiments.

At the faster rotation rates, local midlatitude peaks in stability occur where the eddy heat flux converges. It is interesting to compare the GCM results with the predictions of simple models which parameterize the effects of baroclinic eddies on static stability. Stone (1972, 1973) uses the Eady model to determine stability at 45° latitude, given the static stability of the radiative equilibrium state. His model predicts stability increasing with rotation, which is generally observed at 45° in the GCM (Table 1). The agreement is very good at short periods, where the dynamics is clearly in the baroclinic regime and the beta effects left out of Stone's model are unimportant (because the Rhines radius exceeds the Rossby radius of deformation; see Fig. 7). At periods >4 days, the atmosphere switches to a Hadley regime, and Stone's model is no longer applicable; the agreement is predictably worse at these periods.

More recently, it has been proposed that midlatitude static stability is governed by baroclinic adjustment (Stone, 1978; Held, 1982), which keeps isentropic slopes close to the critical slope required for baroclinic instability in a two-layer model. Table 1 also gives the predicted values for this static stability theory at 45° latitude. While this model also correctly predicts stability increasing with rotation rate, it is also too sensitive and greatly underestimates the stabilizing effect at the longer periods. Performing the comparison at the latitude of peak K_E in each experiment, a more appropriate test, gives even worse results: at the longer periods baroclinic adjustment greatly overstabilizes because of the $\tan\theta$ stability dependence combined with the large high latitude gradients at these periods. This suggests that even if baroclinic instability is occurring in these regions, the eddies are too weak to control the thermal structure.

c. *Eddy horizontal scale and dynamic regimes*

Eddy kinetic energy spectra for several of the experiments are presented in Fig. 6. The peak in the spectrum systematically shifts toward lower wavenumbers as rotation rate decreases, reaching wavenumber 1 at a period of 8 days. This is consistent with indirect estimates of the spectrum for Venus (Travis, 1978; Del Genio and Rossow, 1982) and with general expectations from previous models (Rossow and Williams, 1979).

TABLE 1. Rotation dependence of GCM tropospheric mean Northern Hemisphere static stability (K km^{-1}) at 45° latitude compared with the prediction of the radiative–dynamical equilibrium model of Stone (1972) for a temperature of 250 K and a radiative relaxation time of 0.14 years. Also shown is a prediction at 45° from the baroclinic adjustment model of Stone (1978), assuming dynamic heating which extends over a scale height.

Rotation period (d)	GCM	Stone (1972)	Stone (1978)
2/3	5.4	5.5	4.8
1	5.8	5.6	4.6
2	5.6	5.2	3.8
4	5.0	4.6	3.0
8	4.6	3.9	1.6
16	4.5	3.4	0.5

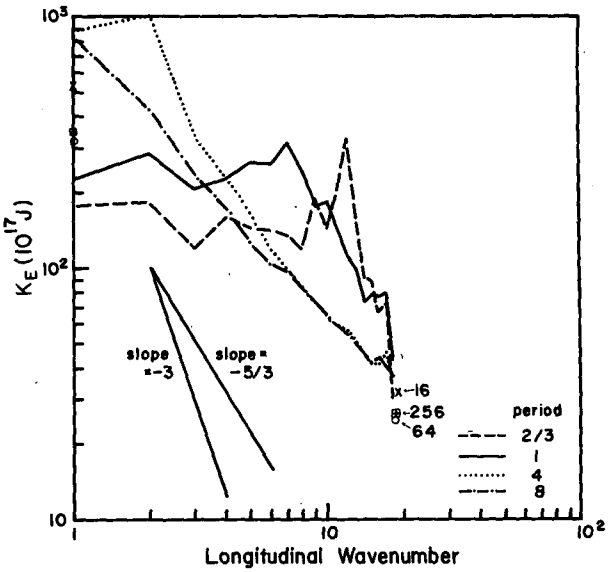

FIG. 6. Tropospheric eddy kinetic energy spectra for several of the experiments. For 16, 64 and 256 days period, the spectral peak is at $n = 1$ and the slope is roughly constant; symbols indicate the power at $n = 1$ and $n = 18$ for these experiments.

Disagreement exists, however, over what determines the preferred horizontal scale of large-scale eddies. The question should really be addressed separately for the rapidly and slowly rotating regimes, in which different eddy processes appear to dominate. The Eady model of baroclinic instability predicts maximum growth at scales proportional to the Rossby radius of deformation NH/f, where N is the Brunt–Väisälä frequency, H is the vertical scale, and f is the Coriolis parameter. Large-scale turbulence studies (Rhines, 1975) have shown that when forcing is weak and inertial effects dominate, energy cascades from the forcing scale up to a larger scale, proportional to $(u/\beta)^{1/2}$, where u is the zonal wind and β the latitudinal gradient of f. The same length also arises from simple scaling of the Rayleigh criterion for barotropic instability.

Scale analysis of the governing equations for atmospheric motion shows that dynamic regimes can be conveniently characterized according to the magnitude of certain key dimensionless numbers (cf. Haltiner, 1971, Ch. 3). Several of these numbers are plotted as a function of rotation period in Fig. 7. For this purpose we define the "observed" horizontal length scale in the GCM as the wavelength/2π of the midlatitude spectral peak in K_E, i.e., as $L = a\cos 45°/n$, where a is the planet radius and n the longitudinal wavenumber. The Rossby number Ro is a measure of geostrophy. The ratio of vertical to horizontal potential temperature

contrast is given by the Richardson number Ri in the cyclostrophic regime and by RiRo in the geostrophic regime; for a Hadley cell, these numbers indicate the relative importance of vertical and horizontal heat transport in balancing differential diabatic heating (cf. Gierasch, 1975). The Burger number $B = \mathrm{RiRo}^2$ is the square of the ratio of the deformation radius to the observed horizontal scale; Rh is comparably defined for the nonlinear Rhines scale. Thus, B and Rh indicate the relevant process which sets the eddy horizontal scale, if adjustments are made for proportionality constants [maximum growth rates in the Eady model occur at 0.62 times the deformation radius, and the turbulent cascade in Rhines' model ceases at a scale of $(2u/\beta)^{1/2}$]. The parameters in Fig. 7, along with the energy cycle (Fig. 1), thus allow us to identify distinct rapid and slow rotation regimes, with a transition near 8 days period, as follows.

Rapidly rotating regime (period $\leq$8 days): Ro < 1, leading to quasi-geostrophic dynamics. Horizontal and vertical temperature contrasts are comparable, since RiRo ~ 1, and baroclinic eddies dominate. Furthermore Rh ~ 1 and $B < 1$, so nonlinear effects apparently shift the eddy scale toward low wavenumbers from the forcing (deformation) scale at which energy is injected in the linear theory. Alternatively, the observed scale may be due to stabilization of the shorter baroclinic waves by the eddy heat flux (Gall et al., 1979). Preferential dissipation of the shorter scales is not a factor here because the GISS model contains no explicit diffusion, and because dissipation by surface drag and convective momentum mixing is relatively uniform for $n = 1$–10.

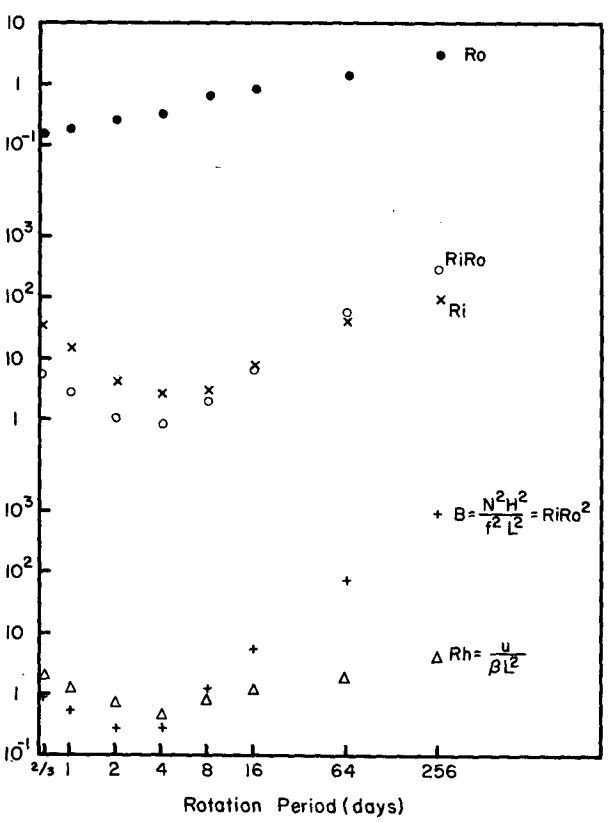

FIG. 7. Characteristic dimensionless numbers at 45°N latitude as a function of rotation period in the experiments.

Slowly rotating regime (period $\geq$8 days): Ro ≥ 1, so the dynamics is not geostrophic. (The flow is too weak to be cyclostrophic except near the midlatitude jet in the 16 day experiment.) Ri $\gg 1$ so horizontal temperature contrasts are small, leading to a quasi-barotropic state dominated by a Hadley circulation. $B \gg 1$ while $n = 1$, i.e., the deformation scale greatly exceeds the size of the planet, so baroclinic instability cannot occur. Instead, a barotropically unstable planetary-scale jet (see section 5) supplies K_E at various scales. Barotropic conversion peaks at wavenumbers 1–3 (Table 2) but Rh > 1. This implies that nonlinear effects determine the scale of the K_E peak but that the cascade is limited ultimately by the size of the planet.

5. Heat and momentum budgets

Latitudinal profiles of dry static energy transport by individual terms in the thermodynamic energy equation are presented for three of the experiments (4, 16, 64 days period) in Fig. 8. In each case the dynamic transport required to balance the differential diabatic heating (sensible plus radiative) is accomplished primarily by the Hadley cell. Transient eddy heat transports are poleward but play a role only at 4 days rotation. Standing eddies transport heat equatorward, reinforcing the Hadley circulation, in all cases.

Quantities related to the angular momentum budget for the same three experiments are shown in Figs. 9, 10 and 11. In each experiment the GCM produces surface easterlies near the equator and surface westerlies elsewhere, requiring net poleward angular momentum transport for their maintenance. Once again the Hadley cell provides most of this transport. The transient and standing eddies contribute significantly at high latitudes at 4 days but oppose the Hadley cell transport at 16 and 64 days.

The behavior of the transient eddy transports is consistent with the idea that they are baroclinic in nature at 4 days period but quasi-barotropic at 16 and 64 days. An effective Prandtl number Pr, defined as the ratio of horizontal eddy momentum and heat diffusivities, can be estimated as

$$\mathrm{Pr} = \frac{F_m}{F_h}\frac{\Delta Q}{\Delta M}, \tag{1}$$

where F_m and F_h are, respectively, the peak zonally averaged transient eddy angular momentum and dry static energy fluxes, and ΔQ and ΔM are, respectively, the equator-pole contrasts in zonal mean heat content (enthalpy) and absolute angular momentum. For the

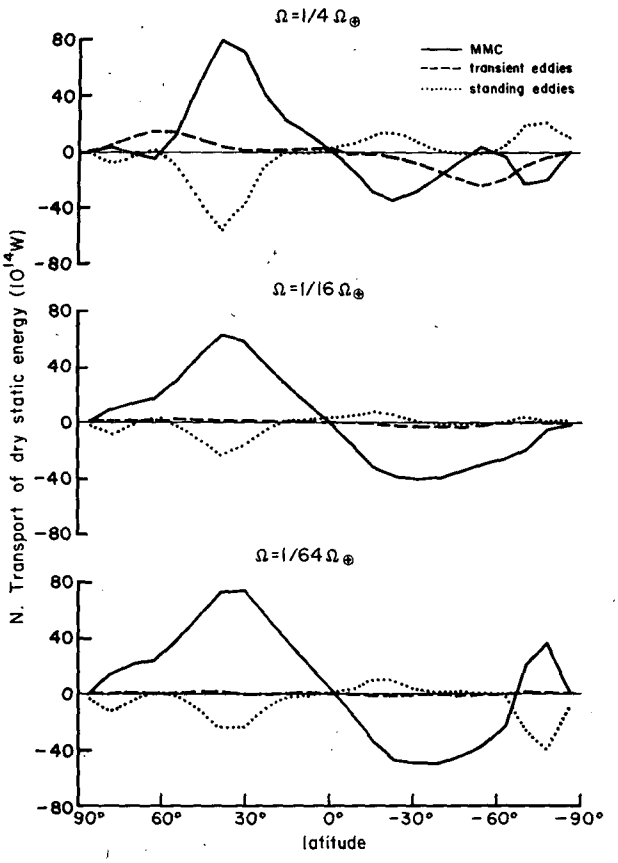

FIG. 8. Latitudinal profiles of vertically integrated northward transport of dry static energy by the mean meridional circulation, transient eddies, and standing eddies for the 4, 16 and 64 day period experiments.

4-day period experiment Pr ~ 0.3, indicating that the eddies transport heat more efficiently than momentum. (Terrestrial experiments with a 4° × 5° version of the GISS GCM suggest that this number may be somewhat resolution-dependent.) The correlation of peak transient eddy heat transport and peak baroclinicity in Fig. 3 is characteristic of a baroclinically unstable disturbance. Eddy angular momentum transport is up the vorticity gradient (Fig. 9), and vorticity increases monotonically with latitude, arguing against the occurrence of barotropic instability (Kuo, 1949).

At 16 and 64 days, on the other hand, transient eddy heat transport is negligible and poorly correlated with the weak temperature gradients (Fig. 3). Eddy angular momentum transports are away from the jet and strongest where jet curvature changes sign (Figs. 10, 11), both of which are predicted by linear barotropic instability theory (Kuo, 1949, 1978). The time mean vorticity field at 16 and 64 days is roughly uniform equatorward of the latitude of maximum shear. Linear theory requires a vorticity extremum to initiate barotropic instability, but the observed vorticity field is more suggestive of the finite amplitude stage in a weakly dissipative atmosphere (cf. Schoeberl and Lindzen, 1984), in which the eddy transports eliminate the extremum and keep the atmosphere close to the critical vorticity gradient. In both of these runs Pr ~ 3, eliminating the possibility of a primarily baroclinically unstable disturbance which also drives some barotropic conversion. By comparison, Rossow (1983) estimated Pr ~ 10 in his Venus GCM.

Despite these arguments, the interpretation at long periods is clouded by the presence of an additional eddy mode. While an order of magnitude larger than in the 4-day experiment and >1, Pr is not large. Furthermore, baroclinic conversion is comparable to or greater than barotropic conversion in all the experiments (Fig. 1). The picture can be clarified by considering Table 2, which shows baroclinic and barotropic conversion as a function of wavenumber at several locations for all three experiments.

At 4 days, positive baroclinic and negative barotropic conversion is restricted to the lowest wavenumbers and is much higher in midlatitudes than at the equator. These appear to be the baroclinically unstable modes. At 16 and 64 days, baroclinic conversion is positive in the global mean but strongly negative at most low wavenumbers in midlatitudes (due to topographic

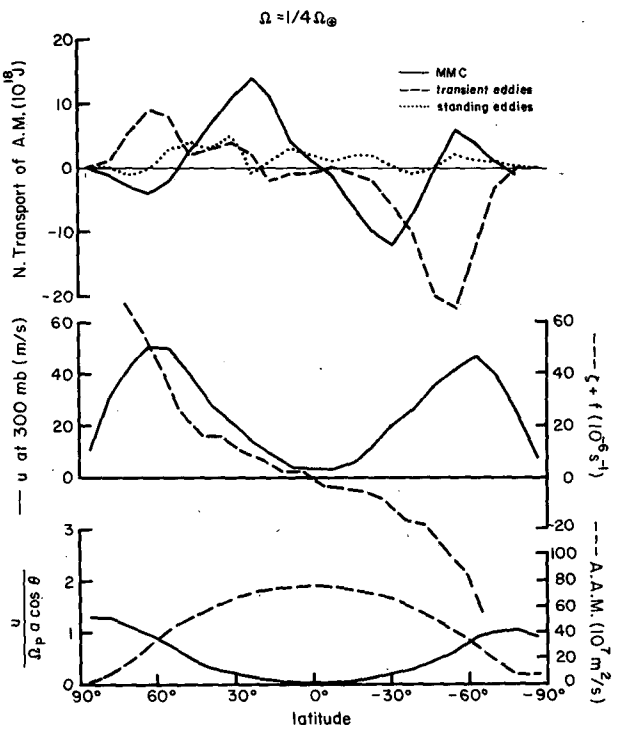

FIG. 9. Zonal mean quantities relevant to the angular momentum budget as a function of latitude for the 4 day period experiment. Top: Vertically integrated northward transport of angular momentum by the mean meridional circulation, transient eddies, and standing eddies. Middle: 300 mb zonal wind (u) and absolute vorticity ($\zeta + f$). Bottom: 300 mb superrotation (Ω_p = planetary angular velocity, a = planetary radius, θ = latitude) and absolute angular momentum.

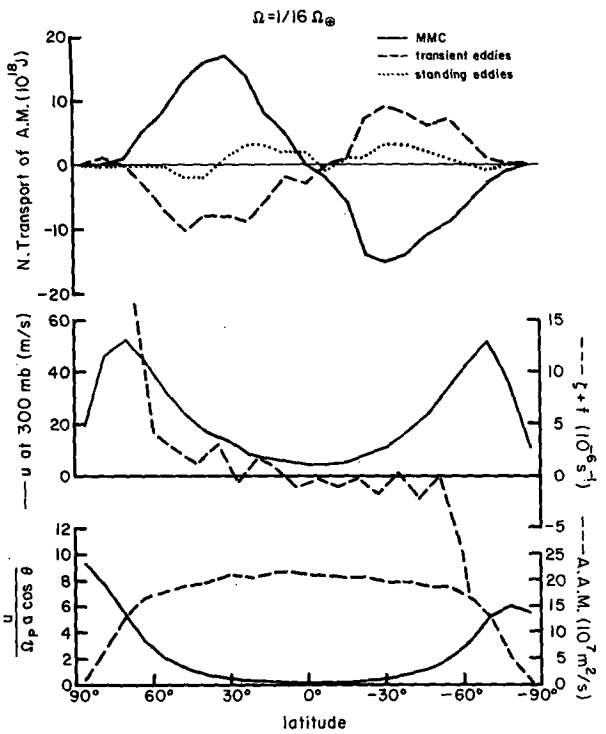

FIG. 10. As in Fig. 9 but for the 16 day period experiment.

forcing), while barotropic conversion is positive everywhere. The latter is concentrated at n = 1–4 with a secondary peak at n = 6–8. It is interesting to note in this regard that Travis (1978) found the *Mariner 10* Venus cloud-tracked wind profile to be linearly barotropically unstable with the largest growth rates at n = 1, 2 and n = 6, 7. Furthermore, the vertical profiles of K_E, u, and eddy momentum transport match, peaking at 300 mb in midlatitudes and 500 mb at high latitudes. By comparison, barotropic conversion is negligible at the equator compared to the strong baroclinic conversion there, especially at n = 1–4. We therefore conclude that quasi-barotropic eddies are indeed dominating the dynamics at middle and higher latitudes, but their effect on the global mean is being overshadowed by other modes at low latitudes.

Vertical heat and momentum budgets for the 4, 16 and 64 day experiments are presented in Fig. 12. In the lowest model layer, sensible heating from the surface is balanced by all the other components of the energy budget, but primarily by convective cooling; both peak near the equator. Radiative and large-scale dynamic cooling play comparable secondary roles, with eddies dominating the dynamic contribution at 4 days and the mean flow dominating at 16 and 64 days. Above this level, radiative cooling is balanced mostly by convection in the middle troposphere and the dominant large-scale dynamic heating term in the upper troposphere.

Vertical eddy transport peaks at 35°N and 20°S, suggesting topographic forcing. A secondary peak occurs at the equator, where land–"ocean" contrasts cause spatial variations of up to 30% in the sensible heat flux and strong baroclinic conversion is observed. Since vertical eddy cooling correlates with surface sensible heating in Fig. 12, it is likely that equatorial waves stimulated by the sensible heat flux pattern represent the additional mode that accounts for the large baroclinic conversion at long periods.

The momentum budget is somewhat simpler. In all three cases, the balance is effectively between upward transport of angular momentum by the mean flow and downward transport by convection at most levels, with eddies playing a very minor role. Surface drag and, to a lesser extent, mountain drag, are important locally in the lowest model level, but their globally averaged contributions are 1–2 orders of magnitude lower than peak local values.

6. Discussion

The issue of superrotation on slowly rotating planets is central to these experiments since they sample both rapidly and slowly rotating regimes. Superrotation, defined here as the ratio of local jet level relative angular velocity to planetary angular velocity, is plotted for the 4, 16 and 64 day cases in Figs. 9, 10 and 11, respectively. Strong superrotation exists at high latitudes in all three

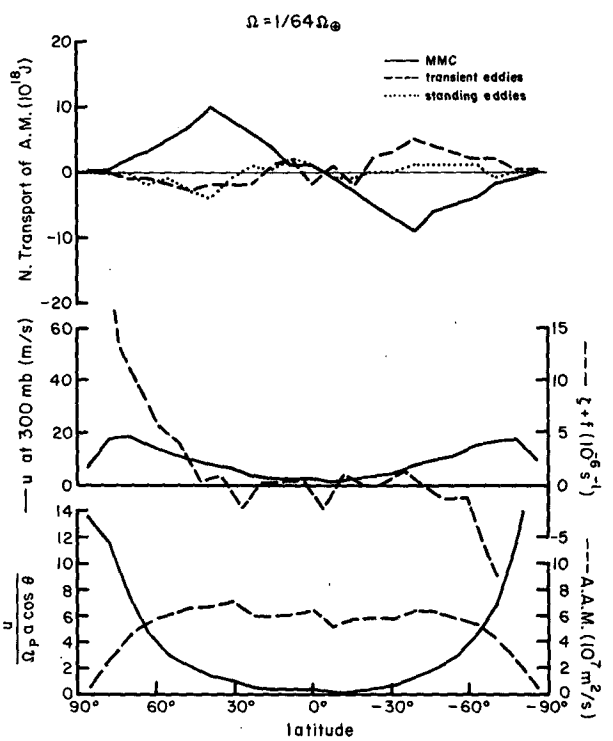

FIG. 11. As in Fig. 9 but for the 64 day period experiment.

TABLE 2. Baroclinic and barotropic conversion (10^{-3} W m^{-2}) as a function of longitudinal wavenumber n for the simulations at three rotation periods.

	Global		45°N		Equator	
n	$\{A\cdot K_E\}$	$\{K_Z\cdot K_E\}$	$\{A\cdot K_E\}$	$\{K_Z\cdot K_E\}$	$\{A\cdot K_E\}$	$\{K_Z\cdot K_E\}$
			4 days			
1	406	−115	1872	−1510	260	−12
2	920	−369	−262	797	175	−4
3	177	−9	−82	283	113	−22
4	130	12	99	11	61	13
5	51	26	118	17	42	1
6	46	13	76	4	10	13
7	47	17	15	47	20	1
8	33	10	36	4	39	0
9	28	15	25	15	10	6
			16 days			
1	36	151	−279	472	237	−3
2	54	93	−53	190	114	4
3	37	42	−21	108	52	−9
4	43	35	−17	74	82	6
5	23	21	40	11	25	3
6	24	12	−6	47	16	−4
7	33	8	25	19	17	−3
8	29	2	17	13	19	−4
9	25	5	28	−2	13	−3
			64 days			
1	53	27	−30	74	193	16
2	67	20	13	63	186	14
3	29	13	−32	61	65	−9
4	43	9	19	2	115	−1
5	10	8	17	8	−4	9
6	9	9	−2	23	36	−14
7	21	3	0	15	26	−12
8	12	7	6	11	7	−3
9	13	5	8	4	−4	6

runs as a result of advection by the Hadley cell. Equatorial superrotation also occurs but is very weak and is not greatly enhanced by the transition from the baroclinic to quasi-barotropic regimes. Failure to generate strong low latitude zonal flow is a common feature of previous slowly rotating Earth experiments as well as the Venus GCM of Rossow (1983). Comparison of the present results with these indicates that equator-pole Hadley cells and equatorward eddy momentum fluxes arising from a barotropically unstable zonal flow are general features of all slowly rotating atmospheres, but that equatorial superrotation is not an inevitable consequence.

In light of this, we must ask why the GCM simulations do not produce the result predicted by Gierasch (1975) and Rossow and Williams (1979) despite the occurrence of the basic eddy–mean flow interaction envisioned by them. The answer can be found by evaluating the criteria for strong superrotation summarized by Gierasch in his analytic model. For this purpose, we consider the 64-day experiment, which is characteristic of the slowly rotating regime. Gierasch's cyclostrophic scaling cannot be used here because of the weak flow at 64 days. However, his criterion on Ri for sufficient vertical stability can be replaced by one on the ratio of vertical to horizontal potential temperature contrast; call this ratio Ri*. In the GCM Ri* $\sim$ 7 in the global mean, so diabatic heating is balanced by adiabatic cooling by the Hadley cell as required. Figure 12, though, suggests that the mean flow is important to the heat budget only at level 3 and above, with convection dominating below. Indeed, the model lapse rate is adiabatic over the first three levels at low latitudes, implying small Ri* there.

The other criteria for the Gierasch mechanism involve comparisons of various dynamic fluxes:

1) Heat transport by the Hadley cell must be unaffected by eddy heat fluxes. (In Gierasch's zonally symmetric calculation, diffusion of heat is in fact not included.) This constraint can be expressed

$$\kappa_H \ll Va\mathrm{Ri}^*, \tag{2}$$

where κ_H is an effective horizontal thermal diffusivity, V is a mean meridional velocity scale, and a is the planetary radius. (This is identical to the first inequality in Gierasch's section 2c.) In the model κ_H, estimated as described in the calculation of Pr, is $\sim 3 \times 10^6$ m^2 s^{-1}, while $V \sim 1.6$ m s^{-1} giving $Va\mathrm{Ri}^* \sim 4 \times 10^7$ m^2 s^{-1}. Thus, transient eddy heat fluxes play no significant role. Standing eddy heat fluxes are slightly stronger but directed equatorward (Fig. 8), thus if anything intensifying the Hadley cell.

2) Poleward angular momentum transport by the Hadley cell must be slower than momentum redistribution by the quasi-barotropic eddies, i.e., the flow must be weakly forced as defined by Rossow and Williams (1979). If ν_H represents an effective horizontal eddy viscosity, this criterion is [see Gierasch's Eq. (17)]

$$\nu_H \gg Va. \tag{3}$$

In the GCM, these two terms are comparable in magnitude ($\sim 10^7$ m^2 s^{-1}), so the flow is not weakly forced. This can also be seen from the ratio of $\{A\cdot K_Z\}$ to $\{K_Z\cdot K_E\}$ (Fig. 1) and from the near uniformity with latitude of absolute angular momentum (Fig. 11) rather than angular velocity equatorward of the jet.

3) Eddy momentum transport must be faster in the horizontal than in the vertical, i.e.,

$$\nu_H \gg \nu_V(a/H)^2, \tag{4}$$

where ν_V is an effective vertical eddy viscosity [also from Eq. (17) of Gierasch]. The parameterized convective momentum mixing in the GCM implies $\nu_V \sim 6 \times 10^3$ m^2 s^{-1}, giving $\nu_V(a/H)^2 \sim 3 \times 10^9$ m^2 s^{-1}. Thus, vertical mixing by small-scale convection dominates horizontal mixing by large-scale eddies, also in conflict with the requirements for the Gierasch mechanism.

4) Meridional overturning must be faster than vertical eddy mixing. The failures of the previous two criteria guarantee that this one too is not satisfied in the GCM.

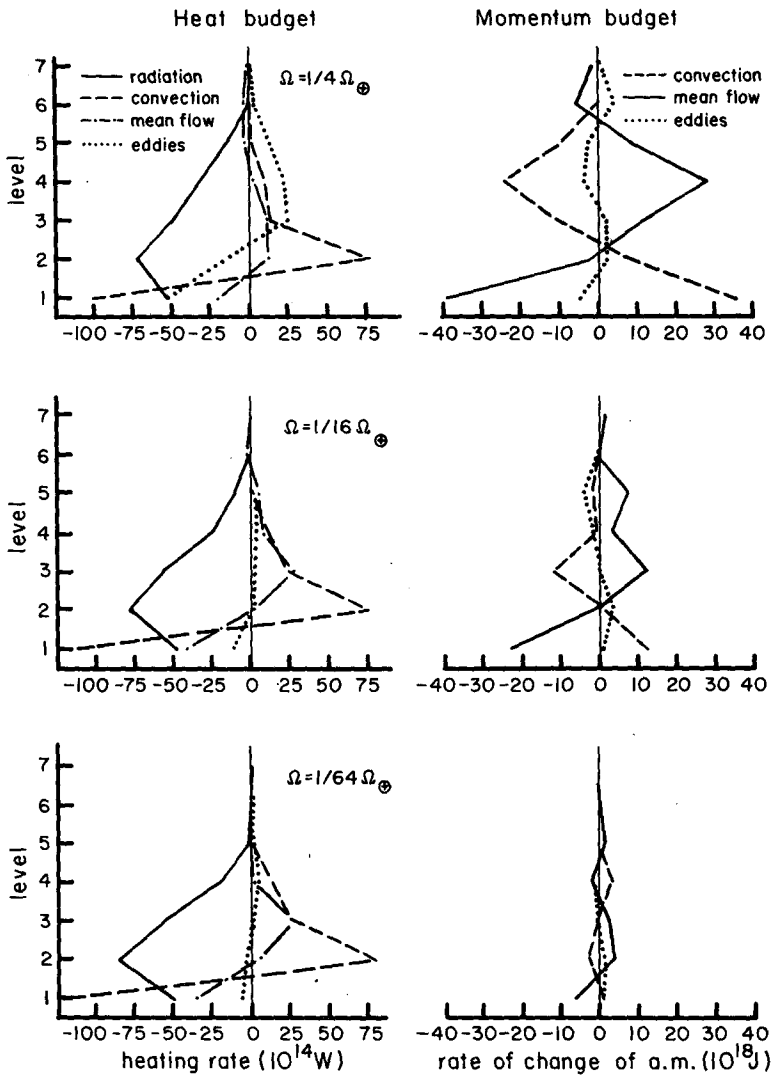

FIG. 12. Horizontally averaged components of the heat and angular momentum budgets as a function of altitude (GCM level) for three of the experiments.

The conditions for the Gierasch mechanism to operate efficiently are therefore not met in the GCM primarily because of the effects of parameterized small-scale convection. Despite the relatively stable radiative state in the model, convection driven by the surface sensible heat flux provides excessive vertical mixing and extends over a significant fraction of the depth of the Hadley cell. This communicates the effects of the surface drag to higher levels and results in a strongly forced flow. Appreciable vertical shear cannot exist, thus limiting the magnitude of upper level zonal winds. These results suggest that the semi-transparency of Earth's atmosphere to solar radiation prevents super-rotation from normally being achieved in slowly rotating Earth models.

Similar arguments can be applied to the Venus GCM of Rossow (1983). His radiative equilibrium state is statically unstable in the lowest 20 km and produces significant low latitude convection at these altitudes, while his surface Hadley cell extends only to 10 km. Thus, his low-level flow is also not weakly forced, giving a flat latitudinal profile of angular momentum similar to that in Fig. 11. Since angular momentum must decrease with latitude in order for a Hadley cell to transport it upward (Gierasch, 1975), Rossow's surface Hadley cell effectively "short-circuits" further transport to higher altitudes, giving a weak upper level jet driven by a locally forced cell. Thus, while attention is usually focused on the Venus cloud level flow, this may be quite sensitive to the details of the lower atmosphere circulation.

If the Gierasch mechanism is to be relevant for Venus, then, a low-level stable layer may be necessary to limit surface-driven convection to a shallow boundary layer and decouple the poleward branch of a lower atmosphere Hadley cell from the surface. Unfortu-

nately, observations of Venus' lower atmosphere are few. However, static stability profiles measured by the *Pioneer Venus* probes (Seiff et al., 1980) were stable from 18 km altitude down to the 12 km level at which the probe temperature sensors failed. *Veneras 9* and *10* (cf. Schubert, 1983) saw a stable layer below ~30 km which extended almost to the surface. These features have not yet been produced in radiative–convective models of Venus, perhaps because of uncertainties in the thermal infrared opacity at these levels, and so are not understood (see Pollack et al., 1980, for a possible explanation). However, the presence of significant vertical shear above ~7 km in zonal winds observed by all Venera and Pioneer Venus probes (cf. Fig. 9 in Schubert, 1983) implies that any thermally driven surface boundary layer is relatively shallow.

By comparison, angular momentum densities inferred from the *Pioneer Venus* day and night probes peak near 20 km (Schubert et al., 1980). By analogy with Earth, this suggests that the poleward branch of the Venus surface Hadley cell occurs at this altitude (Rossow, 1983), well above the implied surface convection level. Rossow also shows that the *Pioneer Venus* probe winds imply solid body rotation up to ~25 km altitude, indicative of efficient equatorward eddy momentum transport and weak forcing.

Of course, the GCM results discussed here do not include the diurnal cycle. The possibility thus exists that the failure of these models to generate large equatorial superrotation is due to the absence of thermal tides. Covey et al. (1986), in fact, interpreted their slowly rotating Earth experiments in this way, although they did not perform an experiment with a diurnal cycle to test the hypothesis. Williams and Holloway (1982) did, but with unrealistically strong diurnal forcing caused by the short terrestrial radiative time scale; their result says less about the role of tides than about the general effect of any eddy process which can rapidly mix angular velocity horizontally. Since radiative relaxation times for disturbances with tidal wavelengths are comparable to the atmospheric rotation period at the Venus cloud tops (Crisp, 1983), it is plausible for the tides to affect the momentum balance there. Vertical transports by other types of gravity waves, such as the Kelvin wave associated with the dark equatorial band in UV images (Covey and Schubert, 1982; Del Genio et al., 1986), may also play a role. In the deep atmosphere, though, radiative time scales are years or more (Stone, 1975) and direct diurnal forcing is probably weak. (Rossow, 1985, discusses a possible exception to this argument.) The Gierasch mechanism is thus a more likely candidate to explain the lower atmosphere angular momentum density peak and solid body rotation profile (as suggested by Rossow, 1985). Likewise, since angular velocity is constant with latitude at depth, it is also possible that this mechanism contributes to the cloud top momentum balance.

Similar implications hold for Titan, which is believed to have a rotation period of 16 days. The 16 day experiment clearly falls into the quasi-barotropic Hadley regime; similar results have been obtained in all other slowly rotating Earth studies. This is consistent with the observed lack of longitudinal temperature contrasts on that planet, which suggests that baroclinic eddies are absent (Flasar et al., 1981). Cyclostrophic winds inferred from observed Voyager latitudinal brightness temperature contrasts by Flasar et al. reach 100 m s^{-1} in midlatitudes in the stratosphere, implying that Titan may superrotate as does Venus. In light of our previous arguments about Venus, it is interesting to note that radio occultation temperature profiles for Titan (Lindal et al., 1983) are dry adiabatic only in the lowest 3.5 km and statically stable above, while a crudely inferred tropospheric Hadley cell (Flasar et al., 1981) extends almost to the tropopause (~50 km). Of course, the possibility of methane moist convection near the surface fed by a mixed ethane–methane ocean of unknown composition (Flasar, 1983) complicates attempts to derive a convective boundary layer depth from the observed temperature profile. However, tidal heating effects are likely to be weaker on Titan than Venus, given its greater distance from the Sun, so *if* superrotation is present, barotropically unstable eddies are clearly the most plausible explanation. On the other hand, the similarity between the shape of the latitudinal temperature profile in our 16-day period experiment (Fig. 3) and that observed in the Titan stratosphere (Flasar et al., 1981, Fig. 2) suggests that *if* Titan is strongly forced, *equatorial* superrotation need not exist, even if strong cyclostrophically balanced *midlatitude* winds are present (see Fig. 4). Determination of the degree of equatorial superrotation on Titan is therefore a key measurement for our understanding of slowly rotating planets.

Figure 7 suggests that the transition from the rapidly to slowly rotating regimes occurs when the midlatitude deformation radius begins to exceed planetary scale (near 8 days period). This is consistent with Hunt's (1979) finding of a baroclinic regime at 5 days period. Actually, the identification of our 4 day period experiment as a baroclinic regime (based on the eddy characteristics) is not clear-cut, since the Hadley cell already dominates the heat transport at this period. Williams and Holloway (1982) and Geisler et al. (1983) actually obtain the transition in eddy behavior at 4 days period. The former, however, could not resolve wavenumbers less than 3 (where most of the eddy energy occurs at 4 days in our results), while the latter used a very weak imposed latitudinal forcing which should suppress baroclinic instability.

If the deformation radius determines the transition period, then the transition depends on the static stability, which is internally determined by the fluid. Since the global mean static stability is independent of rotation in our experiments, we anticipate that in general, the more unstable the radiative equilibrium state, the longer the period at which the transition occurs for a given planetary radius. Thus our results, for a stable

radiative state, probably represent an effective lower limit on the transition period for a planet the size of Earth. We therefore conclude that Titan, which has a small greenhouse effect and small radius, is definitely in the slowly rotating regime. Since $B \sim 5$ for 16 days period (Fig. 7), though, a hypothetical planet with the same period but larger in size and with greater opacity might well fall into the baroclinic regime. On the other hand, B is so large at 256 days period that global baroclinic behavior is probably precluded on Venus despite its large IR opacity and relatively small lower atmosphere static stability.

Although we implicate convection as the cause of negligible superrotation in our and previous models, it is reasonable to ask whether this and other results of the study are sensitive to the horizontal resolution of our GCM. At the terrestrial rotation rate, the GISS 8° × 10° GCM has been shown to be as successful as higher resolution models in reproducing all the important features of Earth's general circulation (Hansen et al., 1983). At longer periods within the baroclinic regime, resolution is less of a factor because K_E peaks at larger scales (Fig. 6), due to the inverse rotation dependence of the deformation radius and Rhines radius. Within the quasi-barotropic regime at the longest periods, all evidence points to wavenumber 1 domination in the fully nonlinear state. Barotropic forcing is well-resolved if the scale is $(u/\beta)^{1/2}$; even if significant forcing occurs at $n = 6$–7, as suggested by Travis (1978), the result should be no worse than that for the terrestrial case, which has forcing at comparable or even smaller scales. Covey et al. (1986, p. 394) in fact obtain results almost identical to ours with a very high resolution (2.5° × 3.5°) GCM; we therefore conclude that our results are not sensitive to model resolution, except perhaps at ⅔ day period.

Vertical resolution is less of an issue here, since our experiments do not include a diurnal cycle and thus do not generate tidal modes with short vertical wavelengths. The seven levels we employ are comparable to most other tropospheric GCMs. It is useful to note, though, that our results are consistent with the more limited experiments of Hunt (1979), who used a model with 18 vertical levels.

7. Conclusions

The failure of previous three-dimensional Venus models to convincingly demonstrate the cause of rapid superrotation on that planet and the expense associated with such models suggest that slowly rotating Earth GCMs should be used as an exploratory tool prior to the design of future Venus GCM simulations. The results of our experiments suggest a number of sensitivity studies which might shed light on the superrotation question and the dynamics of slowly rotating atmospheres in general. It would be useful, for example, to test the model's dynamic response to different vertical profiles of radiative forcing, including cases of weak surface heating and high lower atmosphere stability. A realistic diurnal cycle must be included as an option to test the viability of thermal tides as a forcing mechanism. Since the current model is too dissipative to satisfy the Gierasch requirements, it would be interesting to reduce the efficiency of momentum mixing by small-scale convection in the model. In the same spirit, surface drag coefficients, which are unknown for Venus, should be varied to find the optimum value between the limits of strong drag (which implies strong forcing) and zero drag (which eliminates angular momentum transfer from surface to atmosphere in the absence of topography). Superrotation is clearly not an inevitable consequence of slow rotation, but its possible occurrence on both slowly rotating planets in our solar system suggests that the phenomenon may eventually be reproducible in GCMs under fairly wide ranges of parameter settings.

Acknowledgments. The authors are grateful to M. Allison, C. Covey, R. Opstbaum, D. Rind, W. Robinson, W. Rossow, G. Russell, P. Stone, and L. Travis for helpful discussions and suggestions on the planning of the experiments as well as the manuscript. J. Meccage participated in the early stages of the project as part of the 1983 Summer Institute on Planets and Climate at NASA/GISS. The figures were drafted by J. Mendoza and the final manuscript was typed by D. Alexander, M. Garcia and S. Shively. This work was supported in part by the NASA Planetary Atmospheres Program managed by H. Brinton.

REFERENCES

Arakawa, A., 1972: Design of the UCLA General Circulation Model. Tech. Rep. No. 7, Dept. Meteor., University of California, Los Angeles, 116 pp.

Baker, N. L., and C. B. Leovy, 1987: Zonal winds near Venus' cloud top level: A model study of the interaction between the zonal mean circulation and the semidiurnal tide. *Icarus,* in press.

Counselman, C. C., III, S. A. Gourevitch, R. W. King, G. B. Loriot and E. S. Ginsberg, 1980: Zonal and meridional circulation of the lower atmosphere of Venus determined by radio interferometry. *J. Geophys. Res.*, **85,** 8026–8030.

Covey, C., and G. Schubert, 1982: Planetary-scale waves in the Venus atmosphere. *J. Atmos. Sci.*, **39,** 2397–2413.

——, E. J. Pitcher and J. P. Brown, 1986: General circulation model simulations of superrotation in slowly rotating atmospheres: Implications for Venus. *Icarus,* **66,** 380–396.

Crisp, D., 1983: Radiative forcing of the Venus mesosphere. Ph.D. dissertation, Princeton University, 193 pp.

Del Genio, A. D., and W. B. Rossow, 1982: Temporal variability of ultraviolet cloud features in the Venus stratosphere. *Icarus,* **51,** 391–415.

——, J. T. Lumetta and J. H. Lee, 1986: Evidence for long-term cyclic behavior in Venus equatorial cloud top dynamics. *Bull. Amer. Astron. Soc.*, **18,** 793.

Fels, S. B., and R. S. Lindzen, 1974: The interaction of thermally excited gravity waves with mean flows. *Geophys. Fluid Dyn.*, **6,** 149–191.

Flasar, F. M., 1983: Oceans on Titan. *Science,* **221,** 55–57.

——, R. E. Samuelson and B. J. Conrath, 1981: Titan's atmosphere: Temperature and dynamics. *Nature (London),* **292,** 693–698.

Gall, R., R. Blakeslee and R. C. J. Somerville, 1979: Baroclinic instability and the selection of the zonal scale of the transient eddies of middle latitudes. *J. Atmos. Sci.*, **36,** 767–784.

Geisler, J. E., E. J. Pitcher and R. C. Malone, 1983: Rotating-fluid experiments with an atmospheric general circulation model. *J. Geophys. Res.*, **88,** 9706–9716.

Gierasch, P. J., 1975: Meridional circulation and the maintenance of the Venus atmospheric rotation. *J. Atmos. Sci.*, **32,** 1038–1044.

Golitsyn, G. S., 1970: A similarity approach to the general circulation of planetary atmospheres. *Icarus,* **13,** 1–24.

Goody, R. M., 1964: *Atmospheric Radiation.* Clarendon Press, 436 pp.

Haltiner, G. J., 1971: *Numerical Weather Prediction.* Wiley and Sons, 317 pp.

Hansen, J., G. Russell, D. Rind, P. Stone, A. Lacis, S. Lebedeff, R. Ruedy and L. Travis, 1983: Efficient three-dimensional global models for climate studies: Models I and II. *Mon. Wea. Rev.,* **111,** 609–662.

Held, I. M., 1982: On the height of the tropopause and the static stability of the troposphere. *J. Atmos. Sci.,* **39,** 412–417.

——, and A. Y. Hou, 1980: Nonlinear axially symmetric circulations in a nearly inviscid atmosphere. *J. Atmos. Sci.,* **37,** 515–533.

Hou, A. Y., 1984: Axisymmetric circulations forced by heat and momentum sources: A simple model applicable to the Venus atmosphere. *J. Atmos. Sci.,* **41,** 3437–3455.

Hunt, B. G., 1979: The influence of the Earth's rotation rate on the general circulation of the atmosphere. *J. Atmos. Sci.,* **36,** 1392–1408.

Kuo, H.-L., 1978: A two-layer model study of the combined barotropic and baroclinic instability in the tropics. *J. Atmos. Sci.,* **35,** 1840–1860.

——, 1949: Dynamic instability of two-dimensional and nondivergent flow in a barotropic atmosphere. *J. Meteor.,* **6,** 105–122.

Leovy, C. B., 1985: Zonal winds in the stratosphere of Titan. *The Atmospheres of Saturn and Titan, Proc. Int. Workshop,* Alpbach, Austria, ESA SP-241.

——, 1986: Zonal winds near Venus' cloud top level: An analytic model of the equatorial wind speed. Submitted to *Icarus.*

Limaye, S. S., 1985: Venus atmospheric circulation: Observations and implications of the thermal structure. *Adv. Space Res.,* **5,** 51–62.

Lindal, G. F., G. E. Wood, H. B. Hotz, D. N. Sweetnam, V. R. Eshleman and G.L. Tyler, 1983: The atmosphere of Titan: An analysis of the *Voyager 1* radio occultation measurements. *Icarus,* **53,** 348–363.

Lorenz, E. N., 1960: Generation of available potential energy and the intensity of the general circulation. *Dynamics of Climate,* R. L. Pfeffer, Ed., Pergamon, 86–92.

Newman, M., G. Schubert, A. J. Kliore and I. R. Patel, 1984: Winds in the middle atmosphere of Venus from Pioneer Venus radio occultation data. *J. Atmos. Sci.,* **41,** 1901–1913.

Pechmann, J. B., and A. P. Ingersoll, 1984: Thermal tides in the atmosphere of Venus: Comparison of model results with observations. *J. Atmos. Sci.,* **41,** 3290–3313.

Pollack, J. B., O. B. Toon and R. Boese, 1980: Greenhouse models of Venus' high surface temperature, as constrained by Pioneer Venus measurements. *J. Geophys. Res.,* **85,** 8223–8231.

Read, P. L., 1986a: Super-rotation and diffusion of axial angular momentum: I. "Speed limits" for axisymmetric flow in a rotating cylindrical fluid annulus. *Quart. J. Roy. Meteor. Soc.,* **112,** 231–251.

——, 1986b: Super-rotation and diffusion of axial angular momentum: II. A review of quasi-axisymmetric models of planetary atmospheres. *Quart. J. Roy. Meteor. Soc.,* **112,** 253–272.

Rhines, P. B., 1975: Waves and turbulence on a beta plane. *J. Fluid Mech.,* **69,** 417–443.

Rind, D., and W. B. Rossow, 1984: The effects of physical processes on the Hadley circulation. *J. Atmos. Sci.,* **41,** 479–507.

Rossow, W. B., 1983: A general circulation model of a Venus-like atmosphere. *J. Atmos. Sci.,* **40,** 273–302.

——, 1985: Atmospheric circulation of Venus. *Adv. Geophys.,* **28A,** 347–379.

——, and G. P. Williams, 1979: Large-scale motion in the Venus stratosphere. *J. Atmos. Sci.,* **36,** 377–389.

Schoeberl, M. R., and R. S. Lindzen, 1984: A numerical simulation of barotropic instability. Part I: Wave-mean flow interaction. *J. Atmos. Sci.,* **41,** 1368–1379.

Schubert, G., 1983: General circulation and the dynamical state of the Venus atmosphere. *Venus,* D. M. Hunten, L. Colin, T. M. Donahue, and V. I. Moroz, Eds., University of Arizona Press, 681–765.

——, C. Covey, A. Del Genio, L. S. Elson, G. Keating, A. Seiff, R. E. Young, J. Apt, C. C. Counselman III, A. J. Kliore, S. S. Limaye, H. E. Revercomb, L. A. Sromovsky, V. E. Suomi, F. Taylor, R. Woo and U. von Zahn, 1980: Structure and circulation of the Venus atmosphere. *J. Geophys. Res.,* **85,** 8007–8025.

Seiff, A., D. B. Kirk, R. E. Young, R. C. Blanchard, J. T. Findlay, G. M. Kelly and S. C. Sommer, 1980: Measurements of thermal structure and thermal contrasts in the atmosphere of Venus and related dynamical observations: Results from the four *Pioneer Venus* probes. *J. Geophys. Res.,* **85,** 7903–7933.

Stone, P. H., 1972: A simplified radiative-dynamical model for the static stability of rotating atmospheres. *J. Atmos. Sci.,* **29,** 405–418.

——, 1973: The effect of large-scale eddies on climatic change. *J. Atmos. Sci.,* **30,** 521–529.

——, 1975: The dynamics of the atmosphere of Venus. *J. Atmos. Sci.,* **32,** 1005–1016.

——, 1978: Baroclinic adjustment. *J. Atmos. Sci.,* **35,** 561–571.

Travis, L. D., 1978: Nature of the atmospheric dynamics on Venus from power spectrum analysis of Mariner 10 images. *J. Atmos. Sci.,* **35,** 1584–1595.

Williams, G. P., and J. L. Holloway, Jr., 1982: The range and unity of planetary circulations. *Nature (London),* **297,** 295–299.

Young, R. E., and G. Schubert, 1973: Dynamical aspects of the Venus 4-day circulation. *Planet. Space Sci.,* **21,** 1563–1580.